VIP CO_2 Reduction Very Important Paper

International Edition: DOI: 10.1002/anie.201913198
German Edition: DOI: 10.1002/ange.201913198

Reversible and Selective CO_2 to HCO_2^- Electrocatalysis near the Thermodynamic Potential

*Drew W. Cunningham, Jeffrey M. Barlow, Reyna S. Velazquez, and Jenny Y. Yang**

Abstract: *Reversible catalysis is a hallmark of energy-efficient chemical transformations, but can only be achieved if the changes in free energy of intermediate steps are minimized and the catalytic cycle is devoid of high transition-state barriers. Using these criteria, we demonstrate reversible CO_2/HCO_2^- conversion catalyzed by $[Pt(depe)_2]^{2+}$ (depe = 1,2-bis(diethylphosphino)ethane). Direct measurement of the free energies associated with each catalytic step correctly predicts a slight bias towards CO_2 reduction. We demonstrate how the experimentally measured free energy of each step directly contributes to the < 50 mV overpotential. We also find that for CO_2 reduction, H_2 evolution is negligible and the Faradaic efficiency for HCO_2^- production is nearly quantitative. A free-energy analysis reveals H_2 evolution is endergonic, providing a thermodynamic basis for highly selective CO_2 reduction.*

Introduction

Reversible catalysis between energy storage and utilization reactions has been called a "holy grail" in catalysis,[1] and can only be achieved by levelling the energy landscape of the catalytic cycle. The definitions of bi-direction versus reversible catalysis were recently described.[2] Electrocatalysts that function for both reduction and oxidation reactions are considered bi-directional; however, they are only reversible if they operate at a minimal overpotential in both directions. Reversible reactivity is typically a result of an energy landscape with minimal changes in free energy between intermediates, coupled with low transition-state barriers.

The prototypical example of a reversible electrocatalyst is platinum, which facilitates hydrogen production and oxidation [Eq. (1)] at negligible overpotentials.[3] In nature, hydrogenase enzymes also display reversible electrocatalytic activity and operate near the thermodynamic potential, although different variants display a bias towards either H^+ reduction or H_2 oxidation.[4] More recently, a few synthetic catalysts have achieved reversible $2H^+/H_2$ electrocatalysis.[5]

$$2H^+ + 2e^- \rightleftharpoons H_2 \quad (1)$$

Research in H_2 electrocatalysis is motivated by the prospect of storing renewable electricity in a chemical bond. However, challenges associated with using a gaseous fuel has stimulated interest in applying renewable electricity to recycle CO_2 into liquid fuels.[6] One solution is the reduction of CO_2 to HCO_2^- (formate) [Eq. (2)], a soluble fuel more convenient for storage and transportation.[7] The reverse reaction, electrocatalytic oxidation of formate, is valuable in fuel cells.[7]

$$CO_2 + H^+ + 2e^- \rightleftharpoons HCO_2^- \quad (2)$$

Kang and co-workers recently described the electrocatalytic activity of a bi-directional CO_2/formate electrocatalysis with an iridium pincer compound.[8] Although the compound catalyzes both the reduction and oxidation reaction, the onset potentials are separated by ≈ 1 V. Koper and co-workers described the electrocatalytic activity of Pd–Pt nanoparticles towards CO_2 reduction to formic acid at low overpotentials with a maximum Faradaic efficiency of 88%, with the balance of electrons contributing to H_2 evolution.[9] Electrocatalysis of the reverse reaction, formic acid oxidation, was also observed. However, the Pd–Pt nanoparticle catalyst suffered from deactivation by CO intermediates in both directions. Prior to this work, stable, highly selective reversible catalysis at minimal overpotentials for CO_2 to HCO_2^- interconversion had only ever been observed in two formate dehydrogenase (FDH) enzymes: Mo-dependent FDH from *Escherichia coli* (*Ec*FDH-H)[10] and W-dependent FDH from *Syntrophobacter fumaroxidans*.[11]

Guided by thermodynamic considerations, we describe a selective reversible synthetic electrocatalyst for CO_2/HCO_2^- conversion. Transition-metal-catalyzed CO_2 reduction to formate most commonly proceeds through the following steps: 1) reduction of the resting state complex, 2) protonation to generate a metal-hydride complex, and 3) hydride transfer to form a C–H bond.[12] For a reversible catalyst, formate oxidation follows the microscopic reverse and each step must be close to equilibrium. A prospective catalyst and acid source were selected to minimize the free energy of the third and second step, respectively. Stoichiometric and electrochemical experiments verified chemical and electrocatalytic reversibility. The free-energy change for each chemical step was determined through equilibrium measurements to be ≤ 1 kcal mol^{-1} for a net energy change of 1.1 kcal mol^{-1}, equivalent to a 48 mV overpotential. The experimentally derived energy landscape delineates how the free energies of each step contribute to the catalyst overpotential, illustrating how both catalyst and acid selection are key to minimizing the catalytic overpotential.

The catalyst not only reduces CO_2 to HCO_2^- near the thermodynamic potential, but does so with high selectivity

[*] D. W. Cunningham, J. M. Barlow, R. S. Velazquez, Dr. J. Y. Yang
Department of Chemistry, University of California, Irvine, Natural Sciences II
Irvine, CA 92697 (USA)
E-mail: j.yang@uci.edu
Supporting information and the ORCID identification number(s) for the author(s) of this article can be found under: https://doi.org/10.1002/anie.201913198.

© 2019 Wiley-VCH Verlag GmbH & Co. KGaA, Weinheim

These are not the final page numbers!

(no direct proton reduction to H_2 is observed). Under conditions optimized for reversible catalysis, H_2 evolution is endergonic, leading to high Faradaic efficiency for formate. An analysis of other known transition-metal-hydride complexes capable of CO_2 reduction to formate was also performed. For these complexes, we found that when the acid source is selected to minimize the free energy of protonation (and thus operate at the lowest possible overpotential for the catalyst), H_2 evolution is nearly always endergonic, leading to high selectivity. These results demonstrate how flattening the energy landscape leads to more efficient and more selective catalysis.

Results and Discussion

Catalyst Selection: Reversible CO_2/HCO_2^- Reactivity

The free energy of hydride transfer from a transition-metal hydride to generate HCO_2^- (from CO_2) is described by their hydricities ($\Delta G°_{H-}$) according to Equation (3).[12f,13] Thus, to minimize the free energy for hydride transfer to CO_2, the hydricity of the transition-metal hydride should closely match the hydricity of formate.

$$[MH]^n + CO_2 \rightleftharpoons [M]^{n+1} + HCO_2^-$$
$$\Delta G = \Delta G_{H-}([MH]^n) - \Delta G_{H-}(HCO_2^-) \quad (3)$$

Dubois and co-workers measured the hydricity of $[HPt(depe)_2]^+$ to be 44.2 kcal mol^{-1}[14] and later noted that although $[HPt(depe)_2]^+$ reacts with CO_2 to form sub-stoichiometric amounts of HCO_2^-, $[HPt(depe)_2]^+$ could also be generated by addition of HCO_2^- to $[Pt(depe)_2]^{2+}$.[13a] Based on these observations, it was evident that the hydricity of $[HPt(depe)_2]^+$ is comparable to that of HCO_2^-, although its catalytic activity was not explored.[13a,c] The similar thermodynamic hydricities of $[HPt(depe)_2]^+$ and HCO_2^- makes the former an ideal candidate for reversible reactivity. We previously reported electrocatalytic CO_2 reduction to formate with the related complex $[HPt(dmpe)_2]^{2+}$ (dmpe = 1,2-*bis*(dimethylphosphino)ethane). This variant, with methyl instead of ethyl groups on the phosphorous atom, has a hydricity of 41.4 kcal mol^{-1}.[13c,14b] Hydride transfer to CO_2 for $[HPt(dmpe)_2]^{2+}$ is sufficiently favorable ($\Delta G° = -2.6$ kcal mol^{-1}) that catalysis is not reversible.

The equilibria between the hydride donor/acceptor pairs for the forward ($[HPt(depe)_2]^+/CO_2$) and reverse ($HCO_2^-/[Pt(depe)_2]^{2+}$) reactions provide good starting points to explore the chemical reversibility of the hydride-transfer step. Utilizing previously described synthetic methods, both $[HPt(depe)_2]^+$ and $[Pt(depe)_2]^{2+}$ were isolated. Addition of CO_2 (1 atm) to an acetonitrile solution of $[HPt(depe)_2]^+$ resulted in formation of $[Pt(depe)_2]^{2+}$ in an approximately 16:1 ratio of $[Pt(depe)_2]^{2+}$:$[HPt(depe)_2]^+$ (quantified by $^{31}P\{^1H\}$ NMR spectroscopy, Figure S1). The high solubility of CO_2 at 1 atm in acetonitrile (280 mM CO_2 vs. 20 mM $[HPt(depe)_2]^+$) and the ratio of products leads to an equilibrium constant (K_{eq}) of 1.05(7), which corresponds to a free energy of $\Delta G° = -0.03(4)$ kcal mol^{-1}, Table S1, Scheme 1).

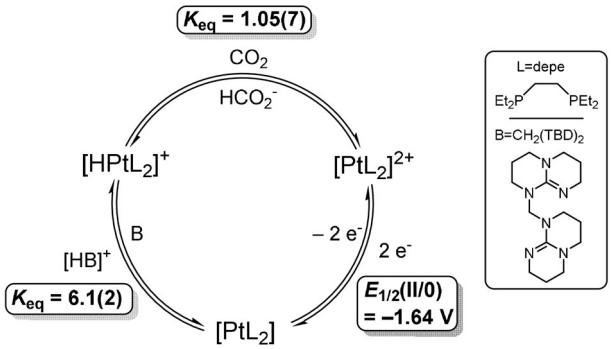

Scheme 1. Proposed catalytic cycle, thermodynamic properties, and abbreviations.

To confirm that hydride transfer between $[HPt(depe)_2]^+$ and CO_2 is at thermodynamic equilibrium, the reverse reaction, hydride transfer from HCO_2^- to $[Pt(depe)_2]^{2+}$, was also investigated. Equilibration of an acetonitrile solution of tetra-*n*-butylammonium formate with an equimolar amount of $[Pt(depe)_2]^{2+}$ under a CO_2 atmosphere yielded identical ratios for $[Pt(depe)_2]^{2+}$/$[HPt(depe)_2]^+$ of 16:1 (Figure S2).

Acid Selection: Protonation/Deprotonation of the Metal Hydride

To generate $[HPt(depe)_2]^+$ for CO_2 reduction, an exogenous acid is required (Scheme 1). Likewise, the microscopic reverse reaction, HCO_2^- oxidation, requires a base to deprotonate $[HPt(depe)_2]^+$. To remain ergoneutral, an acid/base pair with a pK_a value comparable to that of $[HPt(depe)_2]^+$ is required. The pK_a of $[HPt(depe)_2]^+$ was previously reported to be 29.7;[14b] thus, the acid/base pair selected was $CH_2(TBD)_2{\cdot}HPF_6$ (pK_a of 29.0 in acetonitrile) and its conjugate base $CH_2(TBD)_2$ (TBD = triazabicyclodecene; structure shown in Scheme 1).

The stoichiometric deprotonation step between $CH_2(TBD)_2$ with $[HPt(depe)_2]^+$ was quantified by NMR spectroscopy. A J. Young tube containing varying amounts of $[HPt(depe)_2]^+$ and $CH_2(TBD)_2$ was monitored by $^{31}P\{^1H\}$ NMR spectroscopy (Figure S3) to determine the equilibrium constant (K_{eq}) of 6.1(2) ($\Delta G° = -1.07(2)$ kcal mol^{-1}, Table S2, Scheme 1).

Electron Transfer

Completion of the catalytic cycle requires 2 e$^-$ transfer to $[Pt(depe)_2]^{2+}$ (CO_2 reduction) or from $[Pt(depe)_2]$ (HCO_2^- oxidation). The two oxidation states are separated by a reversible two-electron couple at −1.64 V vs. $Fe(C_5H_5)_2^{+/0}$, shown as the grey trace in Figure 1 a.[14]

Reversible Electrocatalysis

The equilibrium studies above demonstrate chemical reversibility of CO_2 to HCO_2^- mediated by $[HPt(depe)_2]^+$. We then sought to demonstrate reversible electrocatalysis.

© 2019 Wiley-VCH Verlag GmbH & Co. KGaA, Weinheim

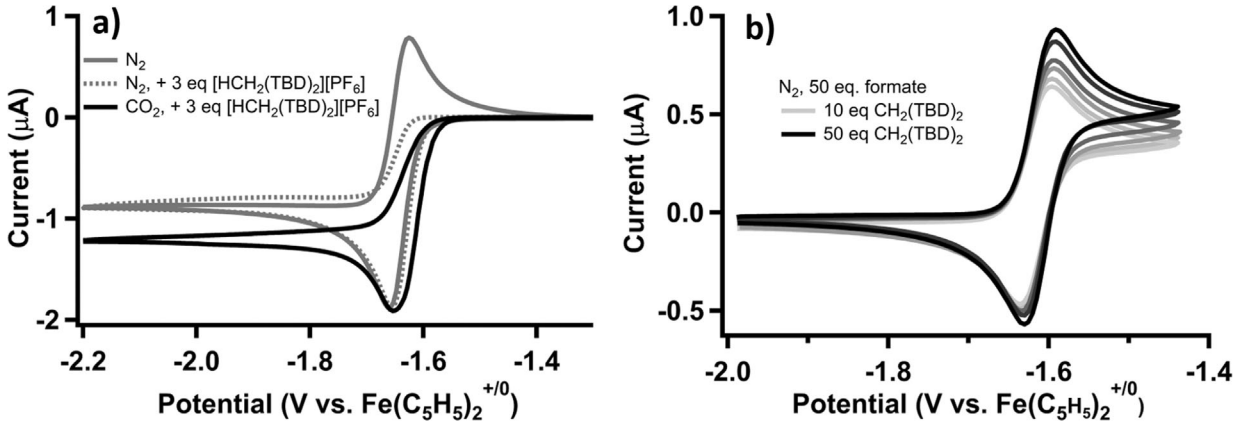

Figure 1. a) Cyclic voltammograms of $[Pt(depe)_2][PF_6]_2$ (1.0 mM) under an atmosphere of dinitrogen (grey trace), under dinitrogen with acid (grey dashed trace), and under an atmosphere of carbon dioxide in the presence of acid (black trace). b) Cyclic voltammograms of $[HPt(depe)_2][PF_6]$ (1.0 mM) under a dinitrogen atmosphere in the presence of $[n\text{-}Bu_4N][HCO_2]$ (50 mM) with concentrations of $CH_2(TBD)_2$ ranging between 10 mM (grey) and 50 mM (black). All scans were recorded in 0.2 M $TBAPF_6$ in acetonitrile at a scan rate of 5 $mV\,s^{-1}$.

Non-equilibrium conditions were used for the cyclic voltammetry experiments to maximize the catalytic response.

CO_2 Reduction

Reduction of $[Pt(depe)_2][PF_6]_2$ by cyclic voltammetry leads to the two-electron reduced product, $[Pt(depe)_2]$ (Figure 1a, grey trace). Addition of the acid, $CH_2(TBD)_2{\cdot}HPF_6$, under 1 atm of N_2 results in protonation after reduction to generate the hydride, $[HPt(depe)_2]^+$ (Figure 1a, dashed grey trace). The extent of protonation depends on the concentration of acid. When 1–2 equivalents of acid are added, some anodic return current is observed, consistent with incomplete protonation, and is expected given the ≈ 1 unit difference in pK_a between the acid and hydride (Figure S4). When three or more equivalents are added (Figure 1a, dashed grey trace), protonation to generate the hydride proceeds to completion; no oxidation event associated with unreacted Pt^0 complex is observed. Cyclic voltammetry of acid titration under 1 atm of CO_2 is shown in Figure S5.

The cyclic voltammetry under 1 atm of CO_2 with 3 equivalents of $CH_2(TBD)_2{\cdot}HPF_6$ is shown as the black trace in Figure 1a. An increase in current is observed, along with the expected loss of reversibility. The increase in current suggests electrocatalytic CO_2 reduction by $[Pt(depe)_2][PF_6]_2$ although the low current enhancement indicates a rate of $< 0.5\ s^{-1}$. The catalytic activity was confirmed by controlled potential electrolysis (CPE). A CO_2-saturated solution of $[Pt(depe)_2][PF_6]_2$ (0.0101 mmol) and $CH_2(TBD)_2{\cdot}HPF_6$ (0.100 mmol) was electrolyzed at -2.0 V vs. $Fe(C_5H_5)_2^{+/0}$ for 5 h. The total amount of charge passed was 11.25 C (Figure S7) for a theoretical maximum amount of formate of 0.058 mmol. ^1H NMR spectroscopy was used to quantify the amount of formate as 0.056 mmol (Figure S8). An internal standard was used in the $^{31}P\{^1H\}$ NMR spectra before and after CPE to verify that the platinum catalyst is completely retained (Figure S9). Additionally, the electrolysis was performed over a pool of mercury, indicating catalysis is not proceeding from the formation of nanoparticles. An equivalent CPE in the absence of catalyst resulted in negligible charge being passed (Figure S7). These results demonstrate $[Pt(depe)_2][PF_6]_2$ is a stable, homogeneous electrocatalyst for the reduction of CO_2 to formate with a TON of 5.5 and Faradaic efficiency of 97%.

Formate Oxidation

The reverse reaction of CO_2 reduction, electrocatalytic formate oxidation, was investigated by cyclic voltammetry (Figure 1b). Titration of 10 to 50 equivalents of base to a solution of $[HPt(depe)_2][PF_6]$ with 50 equivalents of tetra-*n*-butylammonium formate led to an increase in peak current, consistent with electrocatalytic activity with a rate $< 0.5\ s^{-1}$. Since catalysis is reversible, an increase in current is observed for both the anodic and cathodic scans.

Controlled potential electrolysis at -1.4 V vs. $Fe(C_5H_5)_2^{+/0}$ of $[Pt(depe)_2][PF_6]_2$ (0.0113 mmol), tetra-*n*-butylammonium formate (0.1 mmol), and $CH_2(TBD)_2$ (0.1 mmol) in acetonitrile resulted in consumption of 0.027 mmol of formate after 4 hours (Figure S11). A total charge of 5.71 C was transferred throughout the electrolysis period (Figure S10), which corresponds a theoretical maximum formate consumption of 0.030 mmol. Throughout the electrolysis period the total amount of platinum species is conserved, as indicated by the $^{31}P\{^1H\}$ NMR spectra taken before and after electrolysis (Figure S12). In addition, the CPE was also performed over a pool of mercury. An electrolysis experiment performed without catalyst under identical conditions resulted in negligible charge passed (Figure S10). Thus, $[Pt(depe)_2][PF_6]_2$ is a stable, homogeneous electrocatalyst for the oxidation of formate with a minimum TON of 2.4 and a Faradaic efficiency of 90% under these conditions.

Determination of Overpotential from Energy Landscape

The electrocatalytic data establish that $[Pt(depe)_2][PF_6]_2$ is a selective electrocatalyst for the reversible conversion from CO_2 to formate. According to the most recent estimate of the

© 2019 Wiley-VCH Verlag GmbH & Co. KGaA, Weinheim

These are not the final page numbers!

standard potential for CO_2/HCO_2^- in acetonitrile, the thermodynamic potential at a pK_a of 29.0 is −1.63 V vs. $Fe(C_5H_5)_2^{+/0}$.[15] The overpotential calculated by using the $E_{1/2}$ value for $[Pt(depe)_2][PF_6]_2$, as described by Appel and Helm,[16] is 10 mV. We note that our controlled potential electrolysis experiments are performed at the potential of maximum current, or "peak current", to generate sufficient product for accurate quantification.

The experimentally measured equilibrium constants of each intermediate step in our proposed catalytic cycle are represented in the energy landscape shown in Figure 2. The

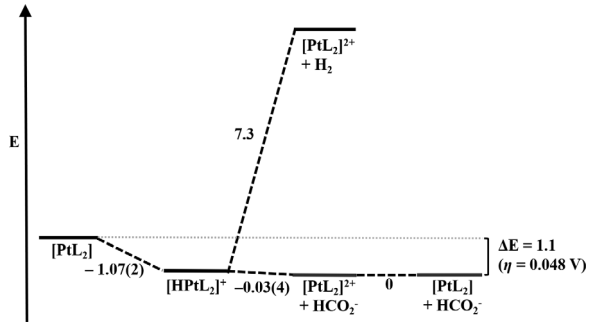

Figure 2. Energy landscape under catalytic conditions (pK_a of 29.0, 1 atm CO_2) at −1.64 V vs. $Fe(C_5H_5)_2^{+/0}$ in CH_3CN. Energetic values are given in kcal mol^{-1} unless otherwise indicated.

energy of protonation of $[Pt(depe)_2]$ to generate $[HPt(depe)_2]^+$, followed by CO_2 addition to form HCO_2^- and $[Pt(depe)_2]^{2+}$ is shown in kcal mol^{-1}. The free-energy diagram is drawn at −1.64 V vs. $Fe(C_5H_5)_2^{+/0}$, or the reversible two-electron couple for $[Pt(depe)_2]^{2+}/[Pt(depe)_2]$. At this potential, the two species are equal in energy. By our measured equilibrium constants, the difference between the initial species and final species varies by −1.1 kcal mol^{-1}, which is equivalent to an overpotential of 0.048 V (1.0 kcal mol^{-1} is equivalent to 0.043 V), slightly higher than expected from the calculation above. A few sources of error are possible with the previously estimated thermodynamic potential. The latter relies on an estimate of the pK_a of formic acid in acetonitrile, which has not been experimentally measured.[17] The calculation also relies on the accuracy of the pK_a of the $CH_2(TBD)_2{\cdot}H^+$ in acetonitrile and the absence of any effects (such as homoconjugation),[18] in which the pK_a would not precisely represent the proton activity of the solution. We note that the overpotential for CO_2 reduction of 0.048 V derived from our energy landscape is from internally consistent equilibrium values and is therefore a more accurate representation of the overpotential. By both calculations, the overpotential is small, as would be expected for a reversible electrocatalyst.

The derivation of the overpotential from the energy landscape depicts an essential tenant of efficient (and reversible) electrocatalysts—intermediate free-energy differences must be minimized. Using a stronger acid than necessary for the protonation step would increase the overpotential by 59 mV, or 1.37 kcal mol^{-1} per excess pK_a unit (consistent with the change in thermodynamic potential for a single proton reaction by the Nernst equation). To illustrate this point, the stronger acid $TBD{\cdot}HPF_6$ (pK_a = 26.0) was also used with this catalyst. Addition of $TBD{\cdot}HPF_6$ to $[Pt(depe)_2]^{2+}$ results in protonation of $[Pt(depe)_2]$ upon reduction of $[Pt(depe)_2]^{2+}$ (black and blue trace in Figure S6). After addition of CO_2 (red trace in Figure S6), no current increase is observed even up to 100 equivalents of $TBD{\cdot}HPF_6$, although the overpotential is now 177 mV larger.

Perhaps less intuitively, using a stronger hydride donor than necessary for CO_2 reduction would also increase the overpotential by 0.043 V per kcal mol^{-1} in excess free energy. Accordingly, it is important in catalyst design to quantify the free energies of bond-making and -breaking steps to make sure they are well matched to achieve a low overpotential.

Product Selectivity and General Applicability

Another noteworthy consequence of minimizing the free energies of intermediate steps is high selectivity for CO_2 reduction in the presence of protons. The free energy of H_2 evolution through protonation of the intermediate metal hydride can be quantified by using the hydricity of the metal hydride, pK_a of the proton source, and the heterolytic bond formation of H_2 (a solvent-dependent constant).[13b,c,19] Although the acid/base pair in the system was selected to match that of the metal hydride to enable reversible catalysis, we find the free energy of H_2 evolution with this acid and the intermediate hydride to be endergonic by 7.3 kcal mol^{-1} (Figure 2). To determine whether this is generally true, we have compiled all metal hydrides with reported hydricity values sufficiently hydridic to reduce CO_2 to formate with measured pK_a values, a total of 17 complexes (Table S3). With only two exceptions, use of external acids that match the pK_a of the metal hydride to minimize the protonation energy results in endergonic H_2 evolution, consequently ensuring catalyst selectivity for CO_2 reduction.

Conclusion

By considering the thermodynamic driving force for each step and avoiding high- and low-energy intermediates we have shown that $[Pt(depe)_2][PF_6]_2$ is an electrocatalyst for both the reduction of CO_2 as well as the oxidation of formate. This represents the first molecular catalyst capable of reversible CO_2/HCO_2^- reactivity.

The equilibrium measurements in this system illustrate the energetic requirements for designing a low overpotential electrocatalyst. Additionally, our approach underscores the importance of quantifying thermodynamic parameters to minimize free energies. These considerations are not unique to this complex and are generally applicable to the design of reversible catalysts. Although the overpotential of this catalyst was minimized, it is kinetically slow, indicating significant transition-state barriers. Thus, thermodynamic considerations are an essential requirement for low overpotential catalysis—but not necessarily sufficient for achieving fast catalysis. Understanding the steps that contribute to the slow kinetics and lowering the respective transition states

 © 2019 Wiley-VCH Verlag GmbH & Co. KGaA, Weinheim

by modifying the catalyst or medium is the next important advancement towards fast, efficient, reversible catalysis.

Acknowledgements

This material is based on work supported by US Department of Energy, Office of Science, Office of Basic Energy Sciences Award DE-SC0012150 and DE-0000243266. R.S.V. gratefully acknowledges support from UCI UROP. J.Y.Y. acknowledges support as a Sloan Foundation Fellow, a Canadian Institute for Advanced Research (CIFAR) Azrieli Global Scholar in the Bio-Inspired Solar Energy Program, and Camille Dreyfus Teacher Scholar.

Conflict of interest

The authors declare no conflict of interest.

Keywords: Carbon dioxide reduction · electrocatalysis · formate · reversible catalysis · thermochemistry

[1] J.-M. Savéant, *ACS Catal.* **2018**, *8*, 7608 – 7611.
[2] V. Fourmond, E. S. Wiedner, W. J. Shaw, C. Léger, *J. Am. Chem. Soc.* **2019**, *141*, 11269 – 11285.
[3] A. Eftekhari, *Int. J. Hydrogen Energy* **2017**, *42*, 11053 – 11077.
[4] a) S. V. Hexter, F. Grey, T. Happe, V. Climent, F. A. Armstrong, *Proc. Natl. Acad. Sci. USA* **2012**, *109*, 11516 – 11521; b) A. Abou Hamdan, S. Dementin, P.-P. Liebgott, O. Gutierrez-Sanz, P. Richaud, A. L. De Lacey, M. Rousset, P. Bertrand, L. Cournac, C. Léger, *J. Am. Chem. Soc.* **2012**, *134*, 8368 – 8371.
[5] a) S. E. Smith, J. Y. Yang, D. L. DuBois, R. M. Bullock, *Angew. Chem. Int. Ed.* **2012**, *51*, 3152 – 3155; *Angew. Chem.* **2012**, *124*, 3206 – 3209; b) N. Priyadarshani, A. Dutta, B. Ginovska, G. W. Buchko, M. O'Hagan, S. Raugei, W. J. Shaw, *ACS Catal.* **2016**, *6*, 6037 – 6049; c) A. Dutta, A. M. Appel, W. J. Shaw, *Nat. Rev. Chem.* **2018**, *2*, 244 – 252.
[6] Z. W. Seh, J. Kibsgaard, C. F. Dickens, I. Chorkendorff, J. K. Nørskov, T. F. Jaramillo, *Science* **2017**, *355*, eaad4998.
[7] a) L. An, R. Chen, *J. Power Sources* **2016**, *320*, 127 – 139; b) T. Vo, K. Purohit, C. Nguyen, B. Biggs, S. Mayoral, J. L. Haan, *ChemSusChem* **2015**, *8*, 3853 – 3858.
[8] J. Bi, P. Hou, P. Kang, *ChemCatChem* **2019**, *11*, 2069 – 2072.
[9] R. Kortlever, I. Peters, S. Koper, M. T. M. Koper, *ACS Catal.* **2015**, *5*, 3916 – 3923.
[10] T. Reda, C. M. Plugge, N. J. Abram, J. Hirst, *Proc. Natl. Acad. Sci. USA* **2008**, *105*, 10654 – 10658.
[11] A. Bassegoda, C. Madden, D. W. Wakerley, E. Reisner, J. Hirst, *J. Am. Chem. Soc.* **2014**, *136*, 15473 – 15476.
[12] a) N. D. Loewen, T. V. Neelakantan, L. A. Berben, *Acc. Chem. Res.* **2017**, *50*, 2362 – 2370; b) A. Taheri, L. A. Berben, *Inorg. Chem.* **2016**, *55*, 378 – 385; c) P. Kang, S. Zhang, T. J. Meyer, M. Brookhart, *Angew. Chem. Int. Ed.* **2014**, *53*, 8709 – 8713; *Angew. Chem.* **2014**, *126*, 8853 – 8857; d) P. Kang, C. Cheng, Z. Chen, C. K. Schauer, T. J. Meyer, M. Brookhart, *J. Am. Chem. Soc.* **2012**, *134*, 5500 – 5503; e) S. Roy, B. Sharma, J. Pécaut, P. Simon, M. Fontecave, P. D. Tran, E. Derat, V. Artero, *J. Am. Chem. Soc.* **2017**, *139*, 3685 – 3696; f) B. M. Ceballos, J. Y. Yang, *Proc. Natl. Acad. Sci. USA* **2018**, *115*, 12686 – 12691; g) R. Kanega, N. Onishi, L. Wang, Y. Himeda, *ACS Catal.* **2018**, *8*, 11296 – 11301; h) J. M. Barlow, J. Y. Yang, *ACS Cent. Sci.* **2019**, *5*, 580 – 588.
[13] a) D. L. DuBois, D. E. Berning, *Appl. Organomet. Chem.* **2000**, *14*, 860 – 862; b) M. Rakowski Dubois, D. L. Dubois, *Acc. Chem. Res.* **2009**, *42*, 1974 – 1982; c) E. S. Wiedner, M. B. Chambers, C. L. Pitman, R. M. Bullock, A. J. M. Miller, A. M. Appel, *Chem. Rev.* **2016**, *116*, 8655 – 8692; d) B. M. Ceballos, C. Tsay, J. Y. Yang, *Chem. Commun.* **2017**, *53*, 7405 – 7408; e) C. Tsay, B. N. Livesay, S. Ruelas, J. Y. Yang, *J. Am. Chem. Soc.* **2015**, *137*, 14114 – 14121.
[14] a) D. E. Berning, B. C. Noll, D. L. DuBois, *J. Am. Chem. Soc.* **1999**, *121*, 11432 – 11447; b) C. J. Curtis, A. Miedaner, W. W. Ellis, D. L. DuBois, *J. Am. Chem. Soc.* **2002**, *124*, 1918 – 1925.
[15] K. M. Waldie, A. L. Ostericher, M. H. Reineke, A. F. Sasayama, C. P. Kubiak, *ACS Catal.* **2018**, *8*, 1313 – 1324.
[16] A. M. Appel, M. L. Helm, *ACS Catal.* **2014**, *4*, 630 – 633.
[17] M. J. Stirling, G. Sweeney, K. MacRory, A. J. Blacker, M. I. Page, *Org. Biomol. Chem.* **2016**, *14*, 3614 – 3622.
[18] a) V. Fourmond, P.-A. Jacques, M. Fontecave, V. Artero, *Inorg. Chem.* **2010**, *49*, 10338 – 10347; b) J. A. S. Roberts, R. M. Bullock, *Inorg. Chem.* **2013**, *52*, 3823 – 3835.
[19] a) C. Tsay, J. Y. Yang, *J. Am. Chem. Soc.* **2016**, *138*, 14174 – 14177; b) C. Tsay, B. M. Ceballos, J. Y. Yang, *Organometallics* **2019**, *38*, 1286 – 1291.

Manuscript received: October 15, 2019
Accepted manuscript online: December 17, 2019
Version of record online: ■■ ■■, ■■■■

 © 2019 Wiley-VCH Verlag GmbH & Co. KGaA, Weinheim

These are not the final page numbers!

Research Articles

CO_2 Reduction

D. W. Cunningham, J. M. Barlow, R. S. Velazquez, J. Y. Yang* ___ ■■■–■■■

Reversible and Selective CO_2 to HCO_2^- Electrocatalysis near the Thermodynamic Potential

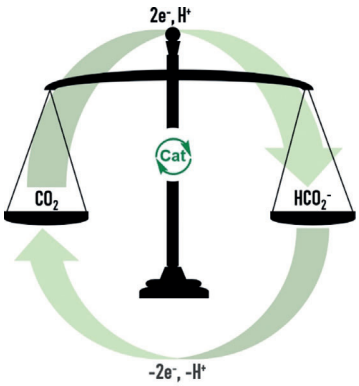

Reversible CO_2 to HCO_2^- conversion is catalyzed by using $Pt(depe)_2][PF_6]_2$ as an electrocatalyst (depe = 1,2-*bis*(diethylphosphino)ethane). High- and low-energy intermediates are avoided by considering the thermodynamic driving force for each step.

© 2019 Wiley-VCH Verlag GmbH & Co. KGaA, Weinheim